Chemical Science

ROYAL SOCIETY OF CHEMISTRY

EDGE ARTICLE

View Article Online
View Journal | View Issue

Cite this: *Chem. Sci.*, 2021, **12**, 14383

All publication charges for this article have been paid for by the Royal Society of Chemistry

Received 31st August 2021
Accepted 2nd October 2021

DOI: 10.1039/d1sc04666g

rsc.li/chemical-science

Synthesis and electronic structure analysis of the actinide allenylidenes, $[\{(NR_2)_3\}An(CCCPh_2)]^-$ (An = U, Th; R = $SiMe_3$)†

Greggory T. Kent, ‡[a] Xiaojuan Yu, ‡[b] Guang Wu,[a] Jochen Autschbach *[b] and Trevor W. Hayton *[a]

The reaction of $[AnCl(NR_2)_3]$ (An = U, Th, R = $SiMe_3$) with *in situ* generated lithium-3,3-diphenylcyclopropene results in the formation of $[\{(NR_2)_3\}An(CH{=}C{=}CPh_2)]$ (An = U, **1**; Th, **2**) in good yields after work-up. Deprotonation of **1** or **2** with LDA/2.2.2-cryptand results in formation of the anionic allenylidenes, [Li(2.2.2-cryptand)][$\{(NR_2)_3\}An(CCCPh_2)$] (An = U, **3**; Th, **4**). The calculated ^{13}C NMR chemical shifts of the C_α, C_β, and C_γ nuclei in **2** and **4** nicely reproduce the experimentally assigned order, and exhibit a characteristic spin–orbit induced downfield shift at C_α due to involvement of the 5f orbitals in the Th–C bonds. Additionally, the bonding analyses for **3** and **4** show a delocalized multi-center character of the ligand π orbitals involving the actinide. While a single–triple–single-bond resonance structure (*e.g.*, An–C≡C–CPh_2) predominates, the An=C=C=CPh_2 resonance form contributes, as well, more so for **3** than for **4**.

Introduction

Despite the significant advancements made in actinide–carbene chemistry in the past decade,[1–6] every example reported thus far has relied on ancillary chelators or heteroatom-containing substituents to stabilize the An–C multiple bond.[7–10] For example, the groups of Ephritikhine and Zi employed a pincer-type ligand to form $[U\{C(PPh_2S)_2\}(BH_4)_2(THF)_2]$ and [Th$\{C(PPh_2S)_2\}_2$(DME), respectively,[11,12] where two thiophosphinoyl pendant arms support the An–carbene interaction. In addition, Liddle *et al.* isolated the silyl-phosphino-carbene [Li(2.2.2-cryptand)][$U\{C(SiMe_3)(PPh_2)\}(BIPM^{TMS})(Cl)$] ($BIPM^{TMS}$ = $C(PPh_2NSiMe_3)_2$), whose U=C bond is stabilized by a P(III) substituent.[13] Similarly, the uranium(IV) arsonium carbene complex $[U(Tren^{TIPS})(CHAsPh_3)]$ ($Tren^{TIPS}$ = $N(CH_2CH_2NSiPr^i_3)_3$) features stabilization by an As(V) substituent.[14] These heteroatom substituents help dissipate the negative charge at the carbene carbon caused by the weak An=C π-bond, which itself results from the energetic mismatch between actinide and carbon valence orbitals combined with the relatively small r_{max} of the 5f orbitals.[14] Without these substituents, the An=C bond would likely be too reactive to isolate.

Because of the requirement for heteroatom substituents, no isolable "Schrock-type" actinide alkylidenes, *i.e.*, An=CR_2 (R = H, alkyl, aryl), are known,[7,9,15] although they have been observed in inert gas matrices.[16–22] Even vinylidene and allenylidene complexes, which should be less reactive than alkylidenes, are unknown, in part due to the lack of viable synthetic routes. Allenylidenes are especially informative in this regard, as they are typically made by H_2O elimination from a propargyl alcohol – a route that is problematic for actinide organometallics given their high sensitivity to water.[23,24]

Herein, we report the synthesis of the actinide allenyl complexes $[\{(NR_2)_3\}An(CH{=}C{=}CPh_2)]$ (An = U, **1**; Th, **2**), formed *via* salt metathesis with lithium-3,3-diphenylcyclopropene. Subsequent deprotonation of **1** and **2** results in the formation of the actinide allenylidene complexes, [Li(2.2.2-cryptand)][$\{(NR_2)_3\}An(CCCPh_2)$] (An = U, **3**; Th, **4**). Significantly, **3** and **4** represent the first complexes with An–C multiple bonds that do not feature heteroatom stabilization.

Synthesis and characterization

Drawing inspiration from the groups of Hashmi and Binger,[25,26] we sought to synthesize an An–cyclopropenyl complex, which we hypothesized could undergo thermal ring opening to form an An–allenyl complex. In fact, addition of *in situ* generated lithium-3,3-diphenylcyclopropene to an Et_2O solution of $[UCl(NR_2)_3]$ (R = $SiMe_3$) does result in formation of the allenyl complex, **1**, which can be isolated as dark-brown blocks in 72% yield after work up (Scheme 1).[25] The thorium analogue **2** can be prepared in a similar fashion in 62% yield, *via* the reaction of $[ThCl(NR_2)_3]$ with 1 equiv. of lithium-3,3-diphenylcyclopropene

[a]*Department of Chemistry and Biochemistry, University of California Santa Barbara, Santa Barbara, CA 93106, USA. E-mail: hayton@chem.ucsb.edu*

[b]*Department of Chemistry, University at Buffalo, State University of New York, Buffalo, NY 14260, USA. E-mail: jochena@buffalo.edu*

† Electronic supplementary information (ESI) available: Experimental procedures, computational results, and spectral data for complexes **1–4**. CCDC 2098903–2098906. For ESI and crystallographic data in CIF or other electronic format see DOI: 10.1039/d1sc04666g

‡ G. T. K. and X. Y. contributed equally to this work.

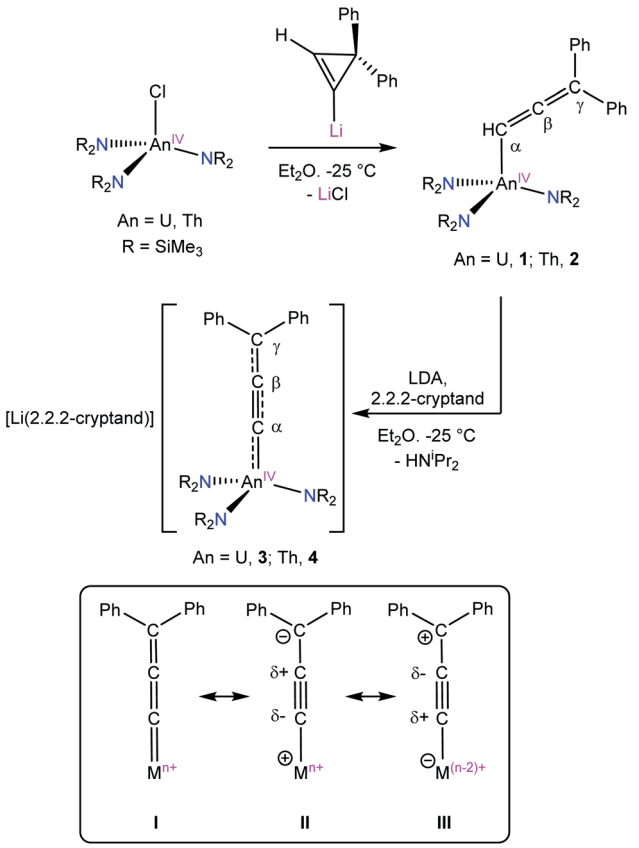

Scheme 1 Synthesis of complexes **1–4**.

in Et_2O. We hypothesize that the ring opening occurs after salt metathesis.

The ^{1}H NMR spectrum of complex **1** in C_6D_6/THF-d_8 features a resonance at −174.8 ppm assigned to the proton attached to the C_α carbon (Fig. S4†). The ^{1}H NMR spectrum of **2** in C_6D_6/THF-d_8 displays a resonance at 5.77 ppm assigned to the same ligand environment (Fig. S5†). Additionally, the $^{13}C\{^1H\}$ NMR spectrum of **2** features resonances at 139.4, 204.7, and 96.7 ppm assigned to the C_α, C_β, and C_γ environments of the allenyl ligand, respectively (Fig. S6†). For comparison, the C_α and C_β NMR shifts of 1,1-diphenylallene are 78.2 and 210.0 ppm, respectively,[27] whereas the C_α, C_β, and C_γ shifts of $[OsCl_2(NO)(CH{=}C{=}CPh_2)(P^iPr_3)_2]$ are 79.1, 199.1, and 101.0 ppm, respectively.[28] We attribute the large C_α shift of **2** to spin–orbit coupling (SOC) effects (see below for more discussion).[4,29–33] Finally, the IR spectra of **1** and **2** exhibit C_α–C_β and C_β–C_γ stretching modes at 1934/1871 and 1934/1869 cm^{-1}, respectively (Table 1). For comparison, $[OsCl_2(NO)(CH{=}C{=}CPh_2)(P^iPr_3)_2]$ exhibits a single C=C stretch at 1881 cm^{-1} in its IR spectrum.[28]

Complexes **1** and **2** both crystallize in the triclinic space group $P\bar{1}$ with one and two independent molecules in their asymmetric unit cells, respectively (Fig. 1). The An–C distances (**1**: 2.457(3); **2**: 2.529(5), 2.536(5) Å) are consistent with those previously reported for An(IV)–C single bonds.[34–37] Additionally, the longer distances observed for **2** reflect the increased ionic radius of Th(IV) *vs.* U(IV) (Table 2).[38] The C_α–C_β and C_β–C_γ distances of the allenyl ligands, along with the C_α–C_β–C_γ angles,

Table 1 Selected IR spectral data for complexes **1–4**

Complex	$\nu(C_\alpha{-}C_\beta)$ (cm^{-1})	$\nu(C_\beta{-}C_\gamma)$ (cm^{-1})
1	1934	1871
2	1934	1869
3	2050	1911
4	2044	1921

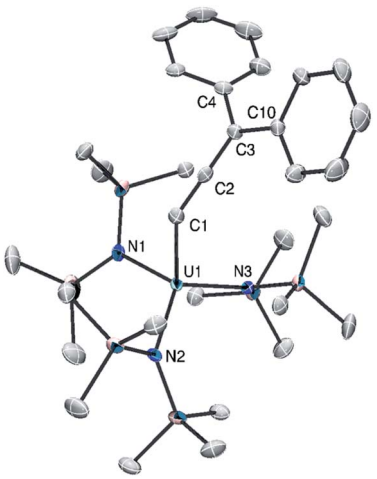

Fig. 1 Solid-state structure of **1** shown with 50% probability ellipsoids. Hydrogen atoms omitted for clarity.

are consistent with those previously reported for transition metal allenyl complexes.[28,39–42] Furthermore, the An–C_α–C_β angles (**1**: 133.2(2); **2**: 132.0(4), 128.6(4)°) confirm that C_α is sp^2 hybridized, consistent with our proposed formulation. Notably, **1** and **2** are the first reported f element allenyl complexes.

Given the low proton affinity at C_α,[43] we hypothesized that addition of base to **1** or **2** would yield an actinide–allenylidene. Gratifyingly, addition of 1 equiv. of LDA and 2.2.2-cryptand to **1** in Et_2O results in the formation of **3**, which can be isolated as dark purple blocks in 54% yield after work-up (Scheme 1). The thorium analogue **4** can be prepared in a similar fashion, *via* the reaction of **2** with 1 equiv. of LDA and 2.2.2-cryptand, in 46% yield as deep orange-red solid. Complexes **3** and **4** are the first reported f-element allenylidenes and are the first An=C complexes that do not employ heteroatoms or ancillary chelators to stabilize the An=C interaction.

The ^{1}H NMR spectrum of **3** in C_6D_6/THF-d_8 features a broad singlet at −1.60 ppm, assignable to the lone $SiMe_3$ environment (Fig. S7†). The ^{1}H NMR spectrum of **4** features a sharp singlet at 0.53 ppm, assignable to its $SiMe_3$ environment (Fig. S7 and S8†), whereas its $^{13}C\{^1H\}$ NMR spectrum exhibits resonances at 205.4, 128.5, and 70.6 ppm. These resonances are assigned to the C_α, C_β, and C_γ environments of the allenylidene ligand, respectively (Fig. S11†). Complexes **3** and **4** exhibit C_α–C_β and C_β–C_γ stretching modes at 2050/1911 and 2044/1921 cm^{-1}, respectively, in their IR spectra (Table 1). These vibrational frequencies are higher than those observed for their respective precursors, suggesting an increase in both the C_α–C_β and C_β–C_γ bond orders upon deprotonation. For further comparison, the

Table 2 Selected metrical parameters for Complexes **1–4**

Bond (Å, °)	**1**	**2**	**3**·C_5H_{12}	**4**·C_5H_{12}
An–C_α	2.457(3)	2.529(5), 2.536(5)	2.305(8)	2.368(16)
C_α–C_β	1.299(4)	1.292(7), 1.288(7)	1.221(11)	1.23(2)
C_β–C_γ	1.329(4)	1.327(7), 1.319(7)	1.403(11)	1.40(2)
C_γ–C_{ipso}	1.490(4), 1.474(4)	1.492(7), 1.487(7), 1.497(7), 1.488(7)	1.443(12), 1.468(12)	1.47(2), 1.45(2)
An–C_α–C_β	133.2(2)	132.0(4), 128.6(4)	173.3(8)	172.0(14)
C_α–C_β–C_γ	176.1(3)	175.5(6), 176.5(6)	176.7(9)	174.6(16)
$\Sigma(\angle C_{ipso/\beta}$–$C_\gamma$–$C_{ipso})$	359.0	360.0/359.9	359.9	359.9

Os allenylidene complex, $[Os(CCCPh_2)(CH_3CN)_3(IPr)(P^iPr_3)][BF_4]_2$, features a single C=C band at 1929 cm^{-1} in its IR spectrum.[44] Finally, the UV-vis spectrum of **4** in C_6H_6 features intense absorptions at 403 nm (ε = 8310 L mol^{-1} cm^{-1}) and 537 nm (ε = 15 030 L mol^{-1} cm^{-1}) (Fig. S12†). The spectrum is qualitatively similar to that recorded for $[CPh_3]^-$,[45] suggesting a similar electronic environment for C_γ (see below for more discussion).

Complexes **3** and **4** crystallize in the monoclinic space group $P2_1$ as the pentane solvates, **3**·C_5H_{12} and **4**·C_5H_{12}, respectively. They are isomorphous and crystallize as discrete cation–anion pairs (Fig. 2). The An–C_α distances in **3** and **4** are 2.305(8) and 2.368(16) Å, respectively (Table 2). These distances are among the shortest known An–C distances and suggest the presence of An–C_α multiple bond character. Additionally, these values are shortened by 0.15 Å from the An–C_α distances observed for their respective precursors. For comparison, the U–C_α distances in $Cp_3U{=}CHPMe_3$ and $[U\{C(SiMe_3)(PPh_2)\}(BIPM^{TMS})(DMAP)_2]$ are 2.274(8) and 2.296(5) Å,[13,46] respectively, whereas the Th–C_α distances in $[(C_5Me_5)_2ThCl(CHPPh_3)]$ and $[Th(CHPPh_3)(NR_2)_3]$ are 2.3235(1) and 2.362(2) Å, respectively.[4,5]

Compared to **1** and **2**, the C_α–C_β distances in **3** and **4** are slightly shortened, whereas the C_β–C_γ distances are slightly elongated. The C_α–C_β distances are similar to those observed for the An–acetylide complexes $[Th(C{\equiv}CH)(NR_2)_3]$ (1.173(12) Å) and $[(NN'_3)U(CCPh)]$ (1.212(5) Å, NN'_3 = $N(CH_2CH_2NSi^tBuMe_2)_3$). However, the An–C distances in these examples are much longer, at 2.481(8) and 2.480(4) Å, respectively, reflecting their single bond character.[47,48] The C_α–C_β–C_γ angles in **3** and **4** remain unchanged, whereas the An–C_α–C_β angles approach linear. In addition, the sum of angles around C_γ confirms that it is sp^2 hybridized (Table 2). These metrical parameters are typical of the allenylidene ligand and can be rationalized by the contribution of resonance forms **I** and **II** to its electronic structure (Scheme 1, inset).[49] For comparison, $[Os(CCCPh_2)(CH_3CN)_3(IPr)(P^iPr_3)][BF_4]_2$ features C_α–C_β and C_β–C_γ distances of 1.246(8) and 1.362(9) Å, respectively.[44]

Electronic structure analysis

The An–allenylidene interaction in complexes **3** and **4** was analyzed *via* relativistic density functional theory (DFT).[50–52,56] Complete computational details and results are provided in the ESI.† Based on Natural Localized Molecular Orbital (NLMO) analyses, complexes **3** and **4** exhibit strong π-delocalization (Fig. 3). Taking **4** as an example, the NLMO picture indicates triple bond character between C_α and C_β, corresponding to resonance structure (RS) **II** in Scheme 1. However, three-center

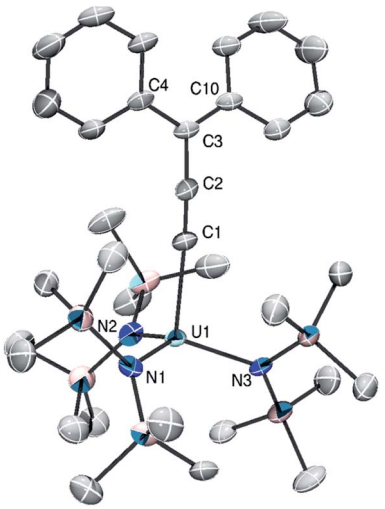

Fig. 2 Solid-state structure of [Li(2.2.2-cryptand)][{$(NR_2)_3$}U($CCCPh_2$)] (**3**) shown with 50% probability ellipsoids. Hydrogen atoms, [Li(2.2.2-cryptand)], and pentane solvate omitted for clarity.

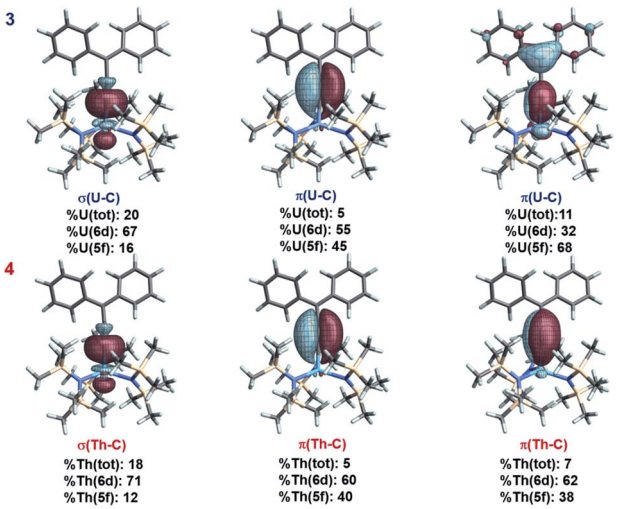

Fig. 3 Isosurfaces (±0.03 a.u.) of selected NLMOs for **3** and **4**. The α spin NLMOs of **3** are shown, weight-% metal character and 6d *vs.* 5f contributions at U are averaged over spins.

character involving thorium, C_α, and C_β, denoted as π(Th–C) in Fig. 3 and Table S1,† also reveals an important contribution from RS **I**. The calculated natural charges for Th, C_α, C_β, and C_γ are 1.52, −0.67, 0.05, and −0.22, respectively, whereas the averaged natural charge for three N atoms bound to Th is −1.65. The NLMO representing the lone pair (and negative charge) at C_γ is π-LP(C_γ), and is strongly delocalized over the phenyl groups, C_β, and even C_α and Th (Fig. S3†). This delocalization further confirms that RS **I** contributes to the overall electronic structure. In addition, for complex **3**, the Mulliken spin population of U is 2.3 (excess alpha over beta spin), beyond the two unpaired spins expected for the f^2 configuration, indicating preferential alpha spin electron donation from ligand to metal. The spin populations for C_α, C_β, and C_γ are −0.08, 0.02, −0.10, respectively; the remaining spin density in the ligand is further delocalized.

An NLMO representing the π-component of a An=C double bond is clearly seen for both **3** and **4** (Fig. 3). This NLMO features multi-center character (**3**: 31% C_α, 28% C_β, and 11% U; **4**: 53% C_α, 37% C_β, and 7% Th), and indicates that RS **I** is an important contributor to the overall electronic structure of both complexes, more so for **3** than for **4**; although the metal weight in **4** is still significant. The other π-bonding NLMO in either complex has only 5% metal weight. Finally, the σ(An–C) bonds of **3** and **4** are represented by two-center two electron NLMOs with 20% and 18% total An weight for **3** and for **4**, respectively (Fig. 3). These results are similar to the weights found in the uranium methanediide complex, $[\{C(PPh_2S)_2\}U(BH_4)_2(THF)_2]$.[12]

As seen in Table S2,† the Wiberg Bond Order (WBO) analyses are consistent with the conclusions drawn from the NLMO picture. For example, the An–C_α, C_α–C_β, and C_β–C_γ WBOs are 0.91, 2.36, and 1.31, respectively, for **4**, and 0.98, 2.40, and 1.28, respectively, for **3**, further suggesting RS **I** is more important for **3** than for **4**. Interestingly, the An–C_α WBOs in **3** and **4** are notably larger than those of **1** (0.60) and **2** (0.57). The An–C_α WBOs in **3** and **4** are also larger than those of the An(IV) parent acetylides, $[An(C{\equiv}CH)(NR_2)_3]$ (An = Th, WBO = 0.67; U, WBO = 0.71).[48] Thus, the larger An–C_α WBOs evident in **3** and **4** *vs.* $[\{(NR_2)_3\}An(CH{=}C{=}CPh_2)]$ *vs.* $[An(C{\equiv}CH)(NR_2)_3]$ also supports the importance of resonance form **I** for these species, and confirms that they can be properly described as actinide carbenes.

An alternative way to examine the bonding in complexes **3** and **4** is offered by the quantum theory of atoms in molecules (QTAIM). This theory utilizes a variety of descriptors based on the topology of the electron density at a bond critical point (BCP).[53] QTAIM data (Table S4†) suggest that the An–C bonds in **3** and **4** are polarised toward the ligand but possess covalent character, and, for **3**, the results are nearly identical to the data reported for $[U(BIPM^{Mes})(Cl)_2(THF)_2]$ ($BIPM^{Mes}$ = $\{C(PPh_2\text{-}NMes)_2\}$).[3] Furthermore, the QTAIM data suggest that Th–C bond in **4** is somewhat less covalent than the U–C bond in **3**, consistent with the NLMO analysis.

^{13}C chemical shift analysis

An NLMO analysis of the ^{13}C NMR shielding for complexes **2** and **4** was performed using the computational methods reported in ref. 50–52 and 54,55,63. Data reported here are from scalar relativistic and spin-orbit (SO) DFT calculations with the PBE functional. Additional data provided in the ESI† show that the calculated shifts do not vary strongly with the functional used in the calculations (Table S3†). We also performed a shielding analysis of allene ($H_2C{=}C{=}CH_2$),[57] for comparison with complex **2**. For all compounds, the diamagnetic and paramagnetic contributions to the shieldings were combined. We confirmed that the observed variations in the carbon shielding and chemical shift come from the (usually negative) paramagnetic shielding mechanism, involving magnetic coupling between occupied and unoccupied orbitals,[58] along with SO effects. The diamagnetic shielding per carbon is essentially constant, as usual. More details are provided in the ESI.†

Our calculated shielding constants for allene agree well with those reported by Wiberg *et al.* who analyzed the system in great detail (Table S3†).[57] Effects from SO coupling (SOC) are very minor, as expected for an organic molecule without a heavy element. C_β is strongly deshielded, by almost 150 ppm, relative to the methylene carbons. The primary reason for this difference is a strong paramagnetic deshielding from both π(C–C) NLMOs for C_β (Table S5†). Although, the σ-bond NLMOs also contribute somewhat to the large shielding difference between the central and terminal carbons.

The calculated chemical shifts for complex **2** agree reasonably well with the experimental data (Tables S3 and S6†). For example, the calculated C_α shift for **2** is 144 ppm (expt. = 139.4 ppm). The replacement of $C_\gamma H_2$ in allene by $C_\gamma Ph_2$ in **2** and the bonding of C_α to Th has a noticeable effect on most of the NLMO shielding contributions, leading to an overall decrease of the C_α and C_γ shielding, relative to allene, and a modest increase (13–17 ppm) of the C_β shielding. The shielding patterns and contributions remain allene-like, however. This conclusion is further buttressed by the WBOs for C_α–C_β (2.0) for C_β–C_γ (1.6). The former value corresponds exactly to the expected bond order, whereas the latter reflects the aforementioned delocalization of π(C_β–C_γ) onto C_{ipso}. The main difference to allene is the inequivalency of C_α and C_γ. The shielding difference is −13 ppm in the calculations without SOC, and is primarily caused by more negative contributions from σ(C_α–Th) and σ(C_α–H) to the C_α shielding *vs.* the σ(C_γ–C_{ipso}) contributions to the C_γ shielding, and a more negative contribution of σ(C_α–C_β) to the C_α shielding *vs.* σ(C_β–C_γ) contributing to the C_γ shielding. These differences are partially counteracted by a more positive allene-like C_α shielding from π(C_α–C_β) compared to the C_γ shielding from π(C_β–C_γ) (Table S6†). The delocalization onto C_{ipso} (Fig. S3†) evidently enhances the C_γ paramagnetic deshielding relative to allene. With SOC effects included, the difference between the C_α and C_γ shielding becomes −39 ppm, as a result of the Th 5f (and 6d) AO contributions in σ(C_α–Th) and an associated SOC deshielding in the C_α core. The situation is reminiscent of the SOC effects on the shielding of nitrogen atoms bound to Th that we identified recently.[59,60]

The calculated ^{13}C chemical shifts for complex **4** (Tables S3 and S7†) also agree reasonably well with the experimental data. For example, the calculated C_α shift for complex **4** is 211 ppm

(expt. = 205.4 ppm). This value includes a 36 ppm deshielding contribution due to SOC, which is about 10 ppm larger in magnitude than that calculated for C_α in complex **2** as a result of the stronger σ(An–C) covalency in **4**. The calculations also reproduce the experimentally assigned chemical shift ordering $C_\alpha > C_\beta > C_\gamma$, in **4**, which is different from complex **2**, for which the shifts are $C_\beta > C_\gamma > C_\alpha$. The increased C_β shielding (smaller chemical shift) in **4** compared to **2** partially reflects the formal C_α–C_β triple bond, according to RS **II**. However, C_β in **4** is still substantially deshielded relative to C_β in an authentic alkyne, such as PhCCH (77.2 ppm chemical shift),[61] consistent with delocalization according to RS **I**. The different ordering is the result of two effects: (1) C_β in **4** has triple bond character with a concomitant increase in magnetic shielding; and (2) the stronger C_α–Th covalency lowers the shielding of C_α in **4**, compared to **2**, *via* the combined effects of greater paramagnetic deshielding due to stronger Th–C bonding, and a stronger SOC deshielding (Tables S6 and S7†). Finally, the SOC induced deshielding for C_β in **4** (−9 ppm) is much larger than that calculated for complex **2** (−4 ppm), which shows independently from the NLMO analysis that the delocalization involves Th, where most of the SOC originates.

Conclusions

In summary, reaction of $[AnCl(NR_2)_3]$ with *in situ* generated lithium-3,3-diphenylcyclopropene affords the first actinide–allenyl complexes, $[\{(NR_2)_3\}An(CH{=}C{=}CPh_2)]$ (An = U, Th). Subsequent treatment with LDA and 2.2.2-cryptand results in the formation of the actinide–allenylidene complexes, $[Li(2.2.2\text{-cryptand})][\{(NR_2)_3\}An(CCCPh_2)]$ (An = U, Th), which represent the first non-heteroatom supported carbene complexes of the actinides. Importantly, their isolation suggests that other actinide cumulenylidene complexes could be isolable, provided a viable synthetic route is available. Quantum chemical calculations give a detailed picture of the actinide–allenylidene interaction, which features partial An=C double bond character. Additionally, the C_α chemical shift in the two Th complexes exhibit SOC-induced deshielding due to 5f orbital participation in the Th–C bonds. The larger deshielding in the allenylidene complex *vs.* the allenyl is consistent with its greater Th–C covalency.

Going forward, we plan to explore the reactivity of our actinide allenylidene for comparison with the late transition metal allenylidenes, which will provide further insight into their electronic structure and potentially uncover new modes of allenylidene reactivity. The latter point is significant because the polarity of the carbon atoms within the actinide allenylidene unit is reversed relative to that observed in the late transition metals (*e.g.*, resonance form **III**, Scheme 1).[23,24,62]

Data availability

Raw experimental and computational data will be made available free of charge upon request.

Author contributions

G. T. K., G. W., and T. W. H. performed the experimental synthesis, characterization, and analysis of the data. X. Y. and J. A. performed the theoretical calculations and analyzed the data. All authors jointly wrote the manuscript. J. A. and T. W. H. secured the funding for the research.

Conflicts of interest

There are no conflicts to declare.

Acknowledgements

This work was supported by the US Department of Energy, Office of Basic Energy Sciences, Chemical Sciences, Biosciences, and Geosciences Division under Contract DE-SC-0001861. J. A. acknowledges support for the theoretical component of this study by the U.S. Department of Energy, Office of Science, Heavy Element Chemistry program, grant DE-SC0001136. We thank the Center for Computational Research (CCR) at the University of Buffalo for providing computational resources.

References

1 S. Fortier, J. R. Walensky, G. Wu and T. W. Hayton, *J. Am. Chem. Soc.*, 2011, **133**, 6894–6897.
2 O. J. Cooper, D. P. Mills, J. McMaster, F. Moro, E. S. Davies, W. Lewis, A. J. Blake and S. T. Liddle, *Angew. Chem., Int. Ed.*, 2011, **50**, 2383–2386.
3 O. J. Cooper, D. P. Mills, J. McMaster, F. Tuna, E. J. L. McInnes, W. Lewis, A. J. Blake and S. T. Liddle, *Chem.–Eur. J.*, 2013, **19**, 7071–7083.
4 D. E. Smiles, G. Wu, P. Hrobárik and T. W. Hayton, *Organometallics*, 2017, **36**, 4519–4524.
5 P. Rungthanaphatsophon, P. Huang and J. R. Walensky, *Organometallics*, 2018, **37**, 1884–1891.
6 P. Rungthanaphatsophon, A. Bathelier, L. Castro, A. C. Behrle, C. L. Barnes, L. Maron and J. R. Walensky, *Angew. Chem., Int. Ed.*, 2017, **56**, 12925–12929.
7 S. T. Liddle, *Angew. Chem., Int. Ed.*, 2015, **54**, 8604–8641.
8 M. Gregson, A. J. Wooles, O. J. Cooper and S. T. Liddle, *Comments Inorg. Chem.*, 2015, **35**, 262–294.
9 T. W. Hayton, *Dalton Trans.*, 2010, **39**, 1145–1158.
10 J. T. Boronski, J. A. Seed, A. J. Wooles and S. T. Liddle, *Chem. Commun.*, 2021, **57**, 5090–5093.
11 W. Ren, X. Deng, G. Zi and D.-C. Fang, *Dalton Trans.*, 2011, **40**, 9662–9664.
12 T. Cantat, T. Arliguie, A. Noël, P. Thuéry, M. Ephritikhine, P. L. Floch and N. Mézailles, *J. Am. Chem. Soc.*, 2009, **131**, 963–972.
13 E. Lu, J. T. Boronski, M. Gregson, A. J. Wooles and S. T. Liddle, *Angew. Chem., Int. Ed.*, 2018, **57**, 5506–5511.
14 J. A. Seed, H. R. Sharpe, H. J. Futcher, A. J. Wooles and S. T. Liddle, *Angew. Chem., Int. Ed.*, 2020, **59**, 15870–15874.
15 M. B. Jones and A. J. Gaunt, *Chem. Rev.*, 2013, **113**, 1137–1198.

16 J. T. Lyon and L. Andrews, *Inorg. Chem.*, 2005, **44**, 8610–8616.
17 J. T. Lyon and L. Andrews, *Inorg. Chem.*, 2006, **45**, 1847–1852.
18 J. Li, H.-S. Hu, J. T. Lyon and L. Andrews, *Angew. Chem., Int. Ed.*, 2007, **46**, 9045–9049.
19 B. O. Roos, R. Lindh, H.-G. Cho and L. Andrews, *J. Phys. Chem. A*, 2007, **111**, 6420–6424.
20 J. T. Lyon, L. Andrews, P.-Å. Malmqvist, B. O. Roos, T. Yang and B. E. Bursten, *Inorg. Chem.*, 2007, **46**, 4917–4925.
21 H.-G. Cho, J. T. Lyon and L. Andrews, *J. Phys. Chem. A*, 2008, **112**, 6902–6907.
22 J. T. Lyon, L. Andrews, H.-S. Hu and J. Li, *Inorg. Chem.*, 2008, **47**, 1435–1442.
23 M. I. Bruce, *Chem. Rev.*, 1998, **98**, 2797–2858.
24 V. Cadierno and J. Gimeno, *Chem. Rev.*, 2009, **109**, 3512–3560.
25 F. F. Mulks, P. W. Antoni, F. Rominger and A. S. K. Hashmi, *Adv. Synth. Catal.*, 2018, **360**, 1810–1821.
26 P. Binger, P. Müller, R. Wenz and R. Mynott, *Angew. Chem., Int. Ed.*, 1990, **29**, 1037–1038.
27 J.-S. Wang, L. Yao, J. Ying, X. Luo and X.-F. Wu, *Org. Chem. Front.*, 2021, **8**, 792–798.
28 H. Werner, R. Fluegel, B. Windmueller, A. Michenfelder and J. Wolf, *Organometallics*, 1995, **14**, 612–618.
29 E. A. Pedrick, P. Hrobárik, L. A. Seaman, G. Wu and T. W. Hayton, *Chem. Commun.*, 2016, **52**, 689–692.
30 A. J. Lewis, P. J. Carroll and E. J. Schelter, *J. Am. Chem. Soc.*, 2013, **135**, 13185–13192.
31 K. C. Mullane, P. Hrobárik, T. Cheisson, B. C. Manor, P. J. Carroll and E. J. Schelter, *Inorg. Chem.*, 2019, **58**, 4152–4163.
32 G. B. Panetti, D.-C. Sergentu, M. R. Gau, P. J. Carroll, J. Autschbach, P. J. Walsh and E. J. Schelter, *Nat. Commun.*, 2021, **12**, 1713.
33 L. A. Seaman, P. Hrobárik, M. F. Schettini, S. Fortier, M. Kaupp and T. W. Hayton, *Angew. Chem., Int. Ed.*, 2013, **52**, 3259–3263.
34 N. S. Settineri, M. E. Garner and J. Arnold, *J. Am. Chem. Soc.*, 2017, **139**, 6261–6269.
35 S. Fortier, B. C. Melot, G. Wu and T. W. Hayton, *J. Am. Chem. Soc.*, 2009, **131**, 15512–15521.
36 L. A. Seaman, J. R. Walensky, G. Wu and T. W. Hayton, *Inorg. Chem.*, 2013, **52**, 3556–3564.
37 A. C. Behrle, A. J. Myers, P. Rungthanaphatsophon, W. W. Lukens, C. L. Barnes and J. R. Walensky, *Chem. Commun.*, 2016, **52**, 14373–14375.
38 R. Shannon, *Acta Crystallogr., Sect. A: Found. Crystallogr.*, 1976, **32**, 751–767.
39 C. J. Elsevier, H. Kleijn, J. Boersma and P. Vermeer, *Organometallics*, 1986, **5**, 716–720.
40 R. S. Keng and Y. C. Lin, *Organometallics*, 1990, **9**, 289–291.
41 A. Wojcicki and C. E. Shuchart, *Coord. Chem. Rev.*, 1990, **105**, 35–60.
42 C. E. Shuchart, R. R. Willis and A. Wojcicki, *J. Organomet. Chem.*, 1992, **424**, 185–198.
43 I. V. Alabugin, in *Stereoelectronic Effects*, 2016, pp. 183–213, DOI: 10.1002/9781118906378.ch7.
44 R. Castarlenas, M. A. Esteruelas, R. Lalrempuia, M. Oliván and E. Oñate, *Organometallics*, 2008, **27**, 795–798.
45 E. Buncel and B. Menon, *J. Org. Chem.*, 1979, **44**, 317–320.
46 R. E. Cramer, M. A. Bruck, F. Edelmann, D. Afzal, J. W. Gilje and H. Schmidbaur, *Chem. Ber.*, 1988, **121**, 417–420.
47 B. S. Newell, A. K. Rappé and M. P. Shores, *Inorg. Chem.*, 2010, **49**, 1595–1606.
48 G. T. Kent, X. Yu, C. Pauly, G. Wu, J. Autschbach and T. W. Hayton, *Inorg. Chem.*, 2021, DOI: 10.1021/acs.inorgchem.1c02064.
49 C. Coletti, A. Marrone and N. Re, *Acc. Chem. Res.*, 2012, **45**, 139–149.
50 J. Autschbach and E. Zurek, *J. Phys. Chem. A*, 2003, **107**, 4967–4972.
51 E. D. Glendening, C. R. Landis and F. Weinhold, *Wiley Interdiscip. Rev.: Comput. Mol. Sci.*, 2012, **2**, 1–42.
52 S. K. Wolff, T. Ziegler, E. v. Lenthe and E. J. Baerends, *J. Chem. Phys.*, 1999, **110**, 7689–7698.
53 R. F. W. Bader, T. S. Slee, D. Cremer and E. Kraka, *J. Am. Chem. Soc.*, 1983, **105**, 5061–5068.
54 J. Autschbach, *J. Chem. Phys.*, 2008, **128**, 164112.
55 J. Autschbach and S. Zheng, *Magn. Reson. Chem.*, 2008, **46**, S45–S55.
56 E. J. Baerends, T. Ziegler, J. Autschbach, D. Bashford, A. Bérces, F. Bickelhaupt, C. Bo, P. Boerrigter, L. Cavallo and D. Chong, 2014, http://www.scm.com.
57 K. B. Wiberg, J. D. Hammer, K. W. Zilm and J. R. Cheeseman, *J. Org. Chem.*, 1999, **64**, 6394–6400.
58 R. V. Viesser, L. C. Ducati, C. F. Tormena and J. Autschbach, *Chem. Sci.*, 2017, **8**, 6570–6576.
59 S. L. Staun, D.-C. Sergentu, G. Wu, J. Autschbach and T. W. Hayton, *Chem. Sci.*, 2019, **10**, 6431–6436.
60 D.-C. Sergentu, G. T. Kent, S. L. Staun, X. Yu, H. Cho, J. Autschbach and T. W. Hayton, *Inorg. Chem.*, 2020, **59**, 10138–10145.
61 B. Wrackmeyer and K. Horchler, *Prog. Nucl. Magn. Reson. Spectrosc.*, 1990, **22**, 209–253.
62 S. W. Roh, K. Choi and C. Lee, *Chem. Rev.*, 2019, **119**, 4293–4356.
63 J. Autschbach, *Mol. Phys.*, 2013, **111**, 2544–2554.